Binder MIMO Channels

Bin Lee, John M. Cioffi, Sumanth Jagannathan, Kibeom Seong, Youngjae Kim, Mehdi Mohseni, and Mark H Brady

Department of Electrical Engineering

Stanford University

Stanford, CA, 94305

Email: {binlee, cioffi, sumanthj, kseong, youngjae, mmohseni, mhbrady}@stanford.edu

Abstract This paper introduces a multiple-input multiple-output (MIMO) channel model for characterization of a binder of telephone lines. This model is based on multiconductor transmission line theory and uses parameters that can be obtained from electromagnetic theory or measured data. The model generates frequency-dependent channel/binder transfer function matrices as a function of cable type, geometric line-spacing and twist-length parameters, and source-load configurations. The model allows extraction of the magnitude and the phase of individual NEXT, FEXT, split-pair, and phantom transfer functions from the transfer function matrix of the binder. These individual crosstalk transfer functions are often found to be very sensitive to small imperfections in the binder. Examples of category 3 twisted pair American telephone lines and “quad” telephone cables appear.

Index Terms— MIMO systems, Crosstalk, Multiconductor transmission lines, Twisted pair cables, Subscriber loops

I. INTRODUCTION

Twisted pair telephone line models in use to date have largely been of an individual line's insertion loss and transfer function. These models have served the DSL and 10/100/G Ethernet communities well. However, with new vectored and/or bonded DSL systems for mitigating and possibly exploiting the crosstalk between multiple lines [1][2], models for a binder of twisted pairs need significant improvement. This paper introduces a multiple-input multiple-output (MIMO) model for telephone lines that allows computation of both the magnitude and phase of all the possible energy transfer functions within a binder, be the direct-line transfer function or the various types of crosstalk. The intent of the model is to enable more accurate and dependable characterization of the various MIMO methods that can be applied to binders of twisted pairs to increase data rates, and in particular to model use of telephone lines for bandwidths of 100s of Megabits per second or possibly even a Gigabit per second, while allowing 100m Category 5e, 6, and 7 transmission of 10Gbps Ethernet data rates (i.e., 10GBASE-T).

The focus of this work will be to extend the well-known Resistance-Inductance-Capacitance-Conductance (RLCG) [3] models for individual twisted pairs to matrix **RLCG** models, and to obtain the necessary parameters for MIMO transmission methods. The matrix **RLCG** models have been examined for general electromagnetic coupling by C. Paul [4], while the steady state solutions for multi-terminal transmission lines were found by Rice [5]. This work focuses on a multiple-twisted pair binder with N pairs or equivalently $2N$ wires. Such a binder has can be modeled by $2N-1$ voltages. When a cable has a shield, there will be 2N+1 conductors and the general theory presented in this paper still applies except that a different geometrical description of cable is needed [6]. This paper introduces load and source matrices, and the potential of matrix-matched load impedances, which is conceptually similar to the single-line case but greatly differs in implementation for MIMO binders. This paper also illustrates the proper extraction of individual NEXT, FEXT, and other interesting transfer functions (like phantom and split-pair transfer functions) from the MIMO matrix model and provides simple explanations of some observed effects in measured NEXT and FEXT.

The limitations of previous research justify this additional work. Past transmission practice within binder cables was based on differential excitation of individual pairs. Thus, channel studies focused on

characterizing wire-pairs under differential excitations. These studies did not treat cable binders as MIMO channels. Nevertheless, previous research generated many interesting results and methods that prepare us for the binder MIMO model of this paper: particularly, methods on modeling twisting for twisted pair cables [7][8], on the importance of cable imperfections [9][10], and empirical power-sum crosstalk characterization [11]. This paper's proposed binder MIMO model extends previous twisting models from single twisting rate per pair to a cable binder comprising lines with different twisting rates, and incorporates cable imperfections. It presents systematic methods to obtain the MIMO channel matrix from basic cable parameters and source-load impedance configurations.

This paper is organized as follows: Section 2 introduces the modeling of $2N$ wires or N pairs. Matrix RLCG models are used to characterize an incremental section following Paul's [4] general treatment of this subject. Terminology is introduced that directly parallels the well-known scalar RLCG models. Section 2 also investigates the appropriate matrix sources and loads and their construction, definition, and relation to traditional N independent differential excitations. An interesting result is that traditional, scalar, differential source and load matching corresponds to an unusual singular situation that is not well-matched in the MIMO case. Section 2 then also lays a foundation for cascades of binder sections that not only allow modeling of traditional gauge changes and "bridged-taps" but also allow modeling of twisting and binder imperfections like twist-rate variation and pair-center-separation variation. Section 3 shows that perfect twisting indeed almost entirely eliminates any crosstalk and that imperfect twisting causes actual measured crosstalk to be several orders larger than what would be produced by perfect twisting. Section 3 also includes a few basic comparisons of actual measured channel transfer characteristics and computed characteristics, providing a strong indication of the model's potential use in modeling of MIMO binder transmission. Section 4 concludes the paper.

II. BINDER MIMO CHANNEL

The goal of the binder MIMO channel model is to obtain channel characteristics for closely packed pairs in a binder. Using MIMO theory, the channel response can be expressed as:

$$\mathbf{Y} = \mathbf{HX} + \mathbf{N}, \tag{1}$$

where **X** is an input column vector, **Y** is an output column vector, and **N** denotes noise components including impulse noise, radio frequency noise, and other background noise. The binder MIMO channel model provides a method to calculate **H** from physical system parameters. The direct-line transfer function, NEXT, and FEXT for the commonly used differential excitation and reception can be easily calculated using **H**.

The binder MIMO channel model uses two concepts: circuit theory and cable geometric modeling. The circuit theory is used to derive voltage-current input-output relations for a cable system. Such derivations require per-unit-length circuit elements that will be provided by cable geometry modeling. This section first presents the circuit theory for a binder MIMO channel, followed by a treatment of the cable geometry modeling.

A. Circuit Theory for a Binder MIMO Channel

The circuit theory for a binder MIMO channel is based on multiconductor transmission line (MTL) theory [4]. This approach elucidates that proper source or load matrices may be more appropriate at both ends of the cable if possible to implement. To apply the theory, a cable loop is treated as a cascade of many segments. Within each segment, the positions of the conductors are fixed, and the positions can vary between segments in order to incorporate twisting and cable imperfections in the model. This subsection first applies MTL theory to a cable segment to obtain voltage-current input-output relations for such a segment; then, the binder MIMO transfer matrix for the system can be calculated for the given source-load configuration. A designer may then cascade sections, multiplying matrix transfer functions to generate the individual NEXT, FEXT, and direct-line transfer functions for the entire binder. This subsection also includes a discussion of split-pair and phantom transfer functions. All these theories assume that certain matrix resistance (**R**), inductance (**L**), capacitance (**C**), and conductance (**G**) values are known for each segment. Models for these matrices appear at the end of this subsection. Methods to obtain **R**, **L**, **C**, and **G** for given geometry configuration are also included.

1) MTL Theory for a Cable Segment

In multiconductor transmission line theory, the small segment of cable shown in Fig. 1(a) can be characterized by matrix parameters **R**, **L**, **C**, and **G**. Four conductor wires are used in the following

discussions for simplicity of illustration. All results and formulae are easily extendable to more wires. In a four-wire cable, one wire can be selected as a common reference; then, the input-output characteristics for the cable can be completely modeled using 3 voltages and 3 currents. To describe this transmission line, 4 incremental resistances, 6 capacitances, 6 inductances, and 6 conductances are required. Fig. 1(a) shows the labeling and indexing of these circuit elements.

The input-output voltage and current relations for a cable segment can be characterized by a transfer matrix $\mathbf{\Phi}$ as in the following formulae:

$$\begin{bmatrix} \mathbf{V}(z,\omega) \\ \mathbf{I}(z,\omega) \end{bmatrix} = \mathbf{\Phi}(z,d,\omega) \begin{bmatrix} \mathbf{V}(z+d,\omega) \\ \mathbf{I}(z+d,\omega) \end{bmatrix}, \tag{2}$$

$$\mathbf{\Phi}(z,d,\omega) = \begin{bmatrix} \mathbf{A}(z,d,\omega) & \mathbf{B}(z,d,\omega) \\ \mathbf{C}(z,d,\omega) & \mathbf{D}(z,d,\omega) \end{bmatrix}, \tag{3}$$

where $\mathbf{V}(z)$ and $\mathbf{I}(z)$ are column vectors, z is the starting position of the cable segment and d is the length of the segment under consideration. **A**, **B**, **C**, and **D** are 3×3 matrices which are functions of the resistance, inductance, conductance, capacitance, the cable geometry and its physical properties. The position and frequency dependence of **A**, **B**, **C**, **D**, **V**, **I**, and $\mathbf{\Phi}$ are explicitly shown in these formulae. The position dependence becomes important when twisting (See Fig. 1(b)) and cable imperfections are included in the model. Due to the position dependence, these matrices will vary from segment to segment. In the rest of the paper, notation for explicit frequency dependence is dropped for convenience. Furthermore, without loss of generality, $z = 0$ is assumed.

In general**,** a cable segment can be described by a position-dependent transmission-line equation. In practical cable systems, **L**, **C**, and **G** are slowly varying with distance along the cable, thus a position-independent transmission line equation can be used for each segment. For channel-modeling purposes, the position-invariant transmission-line equations for each segment are [5][4]:

$$\begin{aligned} -\frac{d\mathbf{V}}{dz} &= (\mathbf{R} + j\omega\mathbf{L})\cdot\mathbf{I} = \mathbf{Z}\cdot\mathbf{I} \\ -\frac{d\mathbf{I}}{dz} &= (\mathbf{G} + j\omega\mathbf{C})\cdot\mathbf{V} = \mathbf{Y}\cdot\mathbf{V} \end{aligned}, \tag{4}$$

where $\boldsymbol{Z} = \boldsymbol{R} + j\omega\boldsymbol{L}$ is the symmetric **per unit length impedance matrix,** and $\boldsymbol{Y} = \boldsymbol{G} + j\omega\boldsymbol{C}$ is the symmetric **per unit length admittance matrix.** The explicit matrix forms of **R, L, C**, and **G** are given in Fig. 1(a). The input-output relation for voltage and current, as well as $\boldsymbol{\Phi}$ can be solved for each segment by extending the well known two-port theory results [12][13]:

$$\begin{bmatrix} \mathbf{V}(0) \\ \mathbf{I}(0) \end{bmatrix} = \begin{bmatrix} \cosh(\boldsymbol{\gamma} d) & \sinh(\boldsymbol{\gamma} d)\cdot \mathbf{Z}_0 \\ \sinh(\boldsymbol{\gamma}^T d)\cdot \mathbf{Z}_0^{-1} & \cosh(\boldsymbol{\gamma}^T d) \end{bmatrix} \cdot \begin{bmatrix} \mathbf{V}(d) \\ \mathbf{I}(d) \end{bmatrix} = \boldsymbol{\Phi}(d) \cdot \begin{bmatrix} \mathbf{V}(d) \\ \mathbf{I}(d) \end{bmatrix}, \tag{5}$$

$$\boldsymbol{\Phi}(d) = \begin{bmatrix} \cosh(\boldsymbol{\gamma} d) & \sinh(\boldsymbol{\gamma} d)\cdot \mathbf{Z}_0 \\ \sinh(\boldsymbol{\gamma}^T d)\cdot \mathbf{Z}_0^{-1} & \cosh(\boldsymbol{\gamma}^T d) \end{bmatrix}, \tag{6}$$

$$\mathbf{Z}_0 = \mathbf{Z}\cdot\boldsymbol{\gamma}^{-\mathbf{T}} = \mathbf{Y}^{-1}\cdot\boldsymbol{\gamma}^{\mathbf{T}} = \boldsymbol{\gamma}^{-1}\cdot\mathbf{Z} = \boldsymbol{\gamma}\cdot\mathbf{Y}^{-1}, \tag{7}$$

$$\mathbf{ZY} = \boldsymbol{\gamma}^2 = (-\boldsymbol{\gamma})^2 = (\mathbf{R} + j\omega\mathbf{L})\cdot(\mathbf{G} + j\omega\mathbf{C}), \tag{8}$$

where $\mathbf{Z}_0$ is the characteristic impedance matrix and $\boldsymbol{\gamma}$ is the propagation constant matrix for the segment. The matrices $\mathbf{Z}_0$ and $\boldsymbol{\gamma}$ are position dependent and vary between segments. The **A**, **B**, **C**, and **D** matrices for one segment, defined in equation (3), can be obtained by a one-to-one mapping with equation (5).

A complete cable can be treated as a cascade of segments both for mathematical convenience and to model a practical cable structure. By modeling a complete cable loop as a cascade of segments, the input-output transfer function for the cable is then:

$$\begin{bmatrix} \mathbf{V}(0) \\ \mathbf{I}(0) \end{bmatrix} = \boldsymbol{\Phi}_1 \cdot \boldsymbol{\Phi}_2 \ldots \boldsymbol{\Phi}_N \cdot \begin{bmatrix} \mathbf{V}(l) \\ \mathbf{I}(l) \end{bmatrix} = \boldsymbol{\Phi} \cdot \begin{bmatrix} \mathbf{V}(l) \\ \mathbf{I}(l) \end{bmatrix}, \tag{9}$$

where $\boldsymbol{\Phi}_i$ describes the input-output transfer function for one segment, l is the length of a full cable, and N is the total number of segments under consideration. If each section of the cable has the same length d, then $l = N \cdot d$. Again, an overall $\boldsymbol{\Phi}$ can be written in terms of the **A**, **B**, **C**, and **D** matrices, which are equal-size square matrices

$$\boldsymbol{\Phi} = \begin{bmatrix} \mathbf{A} & \mathbf{B} \\ \mathbf{C} & \mathbf{D} \end{bmatrix}. \tag{10}$$

Once **A**, **B**, **C**, **D**, and **Φ** are obtained, it is easy to obtain the MIMO channel transfer function as shown in the sequel.

2) MIMO Channel Transfer Function

To calculate the MIMO channel transfer function, an input-output voltage transfer function needs to be calculated. The input-output voltage matrix transfer function **T** for a cable is defined by:

$$\mathbf{V}(l) = \mathbf{T} \cdot \mathbf{V}(0)\ , \tag{11}$$

where $\mathbf{V}(0)$ is the input voltage vector to the cable, and $\mathbf{V}(l)$ is the output voltage vector of the cable. The output voltage vector is related to output current vector by the load admittance matrix $\mathbf{Y}_L$ by

$$\mathbf{I}(l) = \mathbf{Y}_L \cdot \mathbf{V}(l)\ . \tag{12}$$

Using equations (9)-(12), **T** can be computed as

$$\mathbf{T} = \left(\mathbf{A} + \mathbf{B}\mathbf{Y}_L\right)^{-1}. \tag{13}$$

This formula uses the admittance matrix instead of the impedance matrix because the impedance matrix does not exist under the traditional differential load. To get the voltage transfer function between a source and a load, a voltage divider between the source admittance and the input admittance to the cable needs to be considered. The input admittance $\mathbf{Y}_1$ is defined by $\mathbf{I}(0) = \mathbf{Y}_1 \cdot \mathbf{V}(0)$, where $\mathbf{I}(0)$ and $\mathbf{V}(0)$ are the input current and voltage vectors to cable. The formula for the input admittance is given by:

$$\boldsymbol{Y}_1 = \left(\boldsymbol{C} + \boldsymbol{D} \cdot \boldsymbol{Y}_L\right) \cdot \left(\boldsymbol{A} + \boldsymbol{B} \cdot \boldsymbol{Y}_L\right)^{-1}. \tag{14}$$

The transfer function $\mathbf{H}(f)$ between an input voltage supply vector $\mathbf{V}_S$ (with a finite internal series impedance matrix $\mathbf{Z}_S$) and the output voltage $\mathbf{V}_L\ (=\mathbf{V}(d))$ can be calculated by considering $\mathbf{Y}_S$, $\mathbf{Y}_1$ and **T**:

$$\mathbf{H} = \mathbf{T} \cdot \left(\mathbf{Y}_1 + \mathbf{Y}_S\right)^{-1} \cdot \mathbf{Y}_S\ . \tag{15}$$

This formula generates the MIMO channel transfer function **H** as in $\mathbf{Y} = \mathbf{H}\mathbf{X} + \mathbf{N}$ if the input and output are voltage vectors. When one wire is chosen as a common reference in a system with

$2N$ conductor wires, this method produces a $(2N-1)\times(2N-1)$ MIMO channel. The channel derived in this way is referred to as a *Common Mode MIMO channel*. The MIMO channel model works for any source and load admittance ($\mathbf{Y}_S$ and $\mathbf{Y}_L$) (or impedance $\mathbf{Z}_S$ and $\mathbf{Z}_L$) provided the matrix inverses in equations (13), (14), and (15) exist. An interesting choice of load and source impedance matrices is:

$\mathbf{Z}_L = \mathbf{Z}_0(l)$, Load matches the matrix characteristic impedance, or

$\mathbf{Z}_s = \mathbf{Z}_0(0)$, Source matches the matrix characteristic impedance,

where $\mathbf{Z}_0(l)$ is the matrix characteristic impedance of cable at the load end, and $\mathbf{Z}_0(0)$ is the matrix characteristics impedance at the source end.

These matching matrices are particularly meaningful when $\mathbf{Z}_0$ is independent of cable position as for perfect "quad" cables when neighboring quads are neglected[1]. In such cables, load matrix matching completely removes the well-known ripples in NEXT vs. frequency curves. In general, $\mathbf{Z}_L$ and $\mathbf{Z}_s$ in these formulas depend on frequency. However, for real cable systems, $\mathbf{Z}_0$ is almost purely resistive above a few hundred kilohertz. Therefore it is easy to obtain matrix impedance matching at frequencies above a few hundred kilohertz. For twisted pair cable, because $\mathbf{Z}_0$ is position dependent, $\mathbf{Z}_L = \mathbf{Z}_0(l)$ or $\mathbf{Z}_s = \mathbf{Z}_0(0)$ only ensures the load or source impedance matching for either at the load end or source end, but not for whole cable. In general, load matrix matching cannot completely remove ripples in NEXT vs. frequency curves as it does for the "quad" cable. For both the "quad" cable and the twisted pair cable, a simpler load-source configuration is to choose $\mathbf{Z}_L$ and $\mathbf{Z}_s$ to be diagonal matrices.

The common-mode MIMO channel is intuitively the default MIMO channel for a binder cable; but a practical communication system that uses such channel may be complicated to implement and may require sophisticated noise cancellation methods under noisy conditions. A simpler MIMO model for the binder cable exists based on differential excitations and receptions, where sources and loads are individually applied to each pair of conductor wires. The differential excitations and receptions combined with twisting of pairs also significantly reduce crosstalk and noise coupling. In this

[1] "quad" cables are used in France, Germany, and other countries

configuration, FEXT can be defined between pairs and a direct transfer function can be defined for each pair. For a cable system with *N* pairs (or 2*N* wires), a $N \times N$ channel matrix can be defined for such a source-load configuration. In the channel matrix, the direct transfer functions for pairs are in the diagonal positions and FEXT is in the off-diagonal positions. The channel derived in this way is referred to as a *Simplified Differential Mode MIMO Channel*. For example, with four conductor wires forming two differential pairs, the differential mode MIMO channel matrix $\mathbf{H}_{sd}$ is:

$$\mathbf{H}_{sd} = \begin{bmatrix} T_1 & FEXT_{12} \\ FEXT_{21} & T_2 \end{bmatrix}, \tag{16}$$

where T_1 and T_2, are direct transfer functions of each pair, and $FEXT_{12}$ and $FEXT_{21}$ are the FEXT transfer functions induced by one pair to the other pair. In practice, implementing a $N \times N$ differential mode MIMO system is less complicated than implementing a $(2N-1)\times(2N-1)$ common-mode MIMO system. The tradeoff is that the system formed by $2N$ conductor wires has higher channel capacity if the system is modeled as a $(2N-1)\times(2N-1)$ channel rather than an $N \times N$ channel [1][2].

Since the source-load voltage relation is given by matrix transfer function **H**, FEXT as well as NEXT and the direct-line transfer functions can be calculated from **H** under differential loads and sources.

3) Computation of Scalar Direct-line and Crosstalk Transfer Functions with Differential Source and Load Impedances

Fig. 2 illustrates a typical situation where excitations are scalar voltages, and load and source impedances are differential for two lines. Y_p is the admittance of the loads placed across each and every pair, and other quantities are defined by the equations at the bottom of Fig. 2. $\mathbf{Y}_P$ is a 2×2 admittance matrix specified in the figure for the two-port network between wires 2 and 3. The known admittance matrix $\mathbf{Y}_1$ (defined in Fig. 2) can be used to calculate all scalar transfer functions. The basic circuit equation is

$$-\mathbf{Y}_P \cdot \mathbf{V}_P = \mathbf{Y}_{22} \cdot \mathbf{V}_P + \mathbf{Y}_{21} \cdot V_1(1), \tag{17}$$

from which one obtains

$$\mathbf{V}_P = -\left(\mathbf{Y}_P + \mathbf{Y}_{22}\right)^{-1} \cdot \mathbf{Y}_{21} \cdot V_1(1). \tag{18}$$

For a differential source where all pairs use the same source impedance, $Y_P = \begin{bmatrix} \frac{1}{R_S} & -\frac{1}{R_S} \\ -\frac{1}{R_S} & \frac{1}{R_S} \end{bmatrix}$ which is singular. The relation between the scalar source voltage and the network's input voltage is

$$V_S(1) = R_S \cdot I_1(1) + V_1(1) = \left[1 + R_S \cdot y_1\right] \cdot V_1(1), \text{ or} \tag{19}$$

$$V_1(1) = \frac{V_S(1)}{1 + R_S \cdot y_1}. \tag{20}$$

Then, the NEXT transfer function is calculated from (18) and (20) as

$$H_{NEXT} = \frac{V_1(3) - V_1(2)}{V_S(1)} = \begin{bmatrix} -1 & 1 \end{bmatrix} \cdot \frac{\left(\mathbf{Y}_P + \mathbf{Y}_{22}\right)^{-1} \cdot \mathbf{Y}_{21}}{1 + R_S \cdot y_1}, \tag{21}$$

while the matrix transfer function **T** from (13) is additionally used to calculate the FEXT transfer function

$$H_{FEXT} = \frac{V_2(3) - V_2(2)}{V_S(1)} = \begin{bmatrix} 1 & -1 & 0 \end{bmatrix} \cdot \frac{\mathbf{T}}{1 + R_S \cdot y_1} \cdot \begin{bmatrix} -\left(\mathbf{Y}_P + \mathbf{Y}_{22}\right)^{-1} \cdot \mathbf{Y}_{21} \\ 1 \end{bmatrix}, \tag{22}$$

and the main source to load transfer function is

$$H = \frac{V_2(1)}{V_S(1)} = \begin{bmatrix} 0 & 0 & 1 \end{bmatrix} \cdot \frac{\mathbf{T}}{1 + R_S \cdot y_1} \cdot \begin{bmatrix} -\left(\mathbf{Y}_P + \mathbf{Y}_{22}\right)^{-1} \cdot \mathbf{Y}_{21} \\ 1 \end{bmatrix}. \tag{23}$$

The other three NEXT and three FEXT transfer functions can be computed by re-indexing the wires and repeating the procedure. Equations (17)-(20) are valid for any number of lines in which case the quantities $\mathbf{V}_P$, $\mathbf{I}_P$, $\mathbf{Y}_P$, $\mathbf{Y}_{22}$, and $\mathbf{Y}_{21}$ become $(2N-2)$-dimensional. The leading vectors on the right-hand sides of equations (21) and (22) have the two non-zero entries +1 and -1 in the positions of the line into which the crosstalk is being computed. The leading vector in (23) has all zeros except a 1 in the last (right most) position.

These methods to extract information for differential loads from a common-mode MIMO channel matrix can be applied not only to traditional differential excitation, but also to unconventional differential excitations. There are interesting relations among these excitations.

4) Relation to Traditional Models Involving Differential Excitations and "Phantom" Components

Fig. 3 shows 3 views of the same 2-twisted pair cable:

(1) description with all voltages referenced to an external reference (e.g., earth ground) (top)

(2) traditional "symmetric" description using differential excitations and phantom components (left)

(3) asymmetric description of this section that allows direct matrix RLCG models (right) – some of the direct transfer functions are between the wires of different twisted pair, which are sometimes called "split-pair" transfer functions.

The relationship between the models is listed in the figure. The 3 voltages of the traditional symmetric model can be related (input or output) to the 3 voltages of the asymmetric model. The symmetric model includes a 3rd voltage ΔV_p that is often colloquially called a ``phantom'' signal (this name is unfortunate because this voltage exists and can be very real in its effects). The phantom component ΔV_p is defined as: $\Delta V_p = \Delta V_2 - \Delta V_1$. The concept of the phantom component is very useful if one would like to use the 3rd transmission mode, which is available in the asymmetric voltage model, in systems that are already use differential mode transmission. An extra circuit can be implemented on top of the existing differential excitation and reception to utilize this extra mode. For N pairs, $N-1$ phantom modes could be used along with the existing differential mode transmission in order to implement the overall $(2N-1)\times(2N-1)$ MIMO channel, which would otherwise require changing the terminations of existing systems completely. Any transfer functions involving differential and/or phantom components in traditional modeling can always be directly related to transfer functions based on asymmetric voltages and vice versa (Table 1). The two are completely equivalent, and no extra information appears in one with respect to the other (however, some could be easier to measure or use than others in practice). A 4th voltage occurs in the absolute voltage model (top of Fig. 3) and would represent a possible transmission mode with respect to earth ground. However, this mode is not modeled in either symmetric or asymmetric approaches, and is not used in present DSL transmission systems.

The above discussions show that for a cable system with given source-load configuration, if the channel matrix **H** is known, the magnitude and the phase of individual NEXT, FEXT, split-pair and phantom transfer functions can all be calculated. Additionally, for a given source-load configuration, if the **R**, **L**, **C**, and **G** matrices are known for each segment, then the channel matrix **H** can be obtained.

Thus, to complete the model, methods to find the **R**, **L**, **C**, and **G** matrices for each cable segment are needed.

*5) Calculations of the **R**, **L**, **C**, and **G** matrices*

For a given cable geometry, two methods can be used to obtain the per unit length **R**, **L**, **C**, and **G** matrices. One method is based on an analytical approach using basic electromagnetic theory; another method is based on extracting matrix elements from measured data. Calculation of **R**, **L**, **C**, and **G** directly from the basic electromagnetic principle inevitably involves some approximations. Established methods with various levels of approximation can be found in [4][13][14]. One disadvantage of the calculation approach is that it requires knowing the physical constants $\mu, \varepsilon_r, \sigma$ (the permittivity, permeability and conductivity respectively) of the dielectric filling material of cables and the conductivity of metal conductors. These values may not be easy to obtain or to estimate. In addition, the permittivity of the insulation material may also vary across the cable cross-section [23]. The approach based on extracting **R**, **L**, **C**, and **G** from measurements overcomes such difficulties [12]. However, there are drawbacks to this approach. Typically, the frequency-dependent characteristics of a single pair are measured for an isolated twisted pair. In other words, twisted pairs were not in a cable binder, so the measured values are not completely suitable for actual twisted pairs inside a cable binder; therefore, this approach only works as an alternative approximation. In actual simulations, both methods can be implemented, and when some measured data are available one method may be favored over another. Both approaches depend on knowing cable geometric parameters. Therefore, the proposed binder MIMO model includes the following cable geometric models.

B. Cable Geometric Model

To calculate the **R**, **L**, **C**, and **G** matrices, the actual cable geometry needs to be considered. Two types of geometric configurations are discussed in this section: “quad” cables and twisted pair cables. It can be shown theoretically [10][15], and confirmed by simulations in this work, that cable imperfections are important to characterize the channel. So for each type of cable, geometric modeling also contains cable imperfection modeling.

1) Geometric Modeling of Quad Cables

An ideal "single quad" has nice symmetry properties. The four wires in a perfect quad are parallel to each other and the centers of the 4 wires form a square. This symmetry ensures that crosstalk under normal differential excitation is zero when the source and load impedances are setup over one diagonal pair and crosstalk is measured over the other diagonal pair. In real imperfect quads, the centers of the 4 wires do not form a perfect square. Thus, the expected symmetry is imperfect. The quads also rotate along the cable. The rotation does not affect crosstalk characteristics among 4 conductor wires in the same quad, but does reduce crosstalk between different quads much like twisting reduces crosstalk between twisted pairs. A description of the geometry of a single quad requires only the positions of the 4 conductor centers and the conductor radii. Modeling multiple quads within a binder follows the same procedure as described below for twisted pair cables.

2) Geometric Modeling of the Twisted pair Cable

An accurate geometric model of a twisted pair cable is difficult to obtain, therefore, and simplifications are inevitable for the purpose of practical modeling and simulation. This section presents approximations that are used to compare with measurements in this work. These approximations are chosen not only because they are relative simple to implement, but also because simulations based on these approximations reveal typical crosstalk characteristics observed in measurements.

Modeling the geometry of a twisted pair includes a description of the twisting and the associated imperfections. To describe twisting of a pair, the trajectory of the pair center as well as the relative rotations of two wires w.r.t. the pair center are required. Different levels of approximation have been proposed in the past to describe twisting [7][8][16]. For simulation purposes, in this work the single-pair discrete-rotation model [16] is extended to multiple-pair discrete rotation [15], where every pair in a twisted cable is modeled as discretely rotating. The modeling of binder-MIMO imperfections in this work mainly considers three types of cable imperfections: pair center variations, twist-rate variations and non-twisted segment at the cable head or tail. These effects together can be used to model the variation of relative distance between pairs.

a) Type I Imperfection in Twisted pair Cables: Pair Center Variation

The pair-center variation denotes the situation in which the pair centers deviate from the expected position. For an ideal parallel layout of twisted pairs, the centers of any two pairs form parallel straight lines and the distance between the two wire centers in each twisted pair is fixed. This ideal cable is called a "perfect twisted pair cable" in this work. It can be analytically proved that electromagnetic coupling between perfect twisted pairs is almost entirely canceled under normal differential excitation [15]. In reality, because manufacturing procedures are not perfect and twisted pairs are densely packed inside cables, pair centers cannot form straight parallel lines and thus pair center separation varies. In order to model this effect, the centers of the twisted pairs are varied along the cable length, thereby inherently capturing the position dependent separation between the different twisted pairs. The centers of the twisted pairs can be modeled as two-dimensional vectors at each distance z along the cable. The following model applies independently to both components of the pair center vector.

Let $pc(i,z)$ denote any component of the center of pair i along the cable of length z.

$$pc(i,z) = \overline{pc}(i,z) + \Delta pc(i,z), \tag{24}$$

where i is an index for each pair in a twisted pair cable, $\overline{pc}(i,z)$ is the expected pair center position for pair i at the cable of length z and $\Delta pc(i,z)$ is the deviation from the expected position. For non-parallel wires within the cable, $\overline{pc}(i,z)$ can be described by known parameters. In this work, two pair-center variation methods are examined and are used to compare with measurements: a random variation method and a sinusoidal variation method. In the case of random variation,

$$\Delta pc(i,z) = \alpha(i,z) \cdot \overline{pc}_0(i), \tag{25}$$

where $\alpha(i,z)$ is a random function of z. For a practical twisted pair cable structure, it was observed via simulations that the value of $\alpha(i,z)$ is most likely in the range of [0, 0.15]; $\overline{pc}_0(i)$ is the average of the pair center position. For the sinusoidal variation,

$$\Delta pc(i,z) = \alpha_i \sin(k_i \cdot z) \cdot \overline{pc_0}(i), \tag{26}$$

where α_i is a constant for a pair and k_i denotes space frequency. In the case of the single pair discrete rotation model, k_i is a reciprocal of the twist rate tr of the pair. In this paper, the twist rate of a twisted

pair is defined as the average space period of the twisted pair (in the length of meter or inch). For the two pair or the multi-pair discrete-rotation model, k_i can be obtained from the geometric cable structure. Simulations show that $0 < \alpha_i < 0.2$ works for many practical twisted pair cable structures. A few more sophisticated pair-center variation options have been investigated to include the "squeezing" effect from the neighboring pairs, however their improvements were negligible and so are not further considered. The net effect of pair-center variation is that such variation breaks the electromagnetic-coupling cancellation mechanism inside a length of the basic cycle for perfect twisted pairs and thereby increases the electromagnetic coupling between pairs. Equivalently, the pair-center variation increases FEXT to levels that are consistent with those measured in practice. However, pair-center variation alone is not enough to explain the measured NEXT, which necessitates another type of variation, called "twist rate non-uniformity variation."

b) Type II Imperfection in Twisted-Pair Cables: Twist Rate Non-Uniformity Variations

NEXT is proportional to the constructive reflection when the electromagnetic wave travels along a cable. For a twisted pair cable system with a periodic nature of cable geometry, the effective averaging over a basic period of the twisting causes a uniform appearance of the **R**, **L**, **C**, and **G** matrices. Accordingly, the matrix characteristic impedance is uniform. This implies that that although there can be minor reflections of electromagnetic waves inside a section of the cable corresponding to one period, there is not much reflection between such periods. In a real cable, uniformity of the cable is not guaranteed. Consequently, larger section-to-section reflections are often created and lead to the high NEXT levels that are usually observed in measurements. There are a few possible reasons for this "uniformity break": the first reason is the existence of the neighboring pairs. However, simulation results suggest that neighboring pairs do not induce enough reflection. A more likely reason is the twist-rate non-uniformity. The twist-rate is defined as the number of twists per unit meter of the pair. This work uses the following approximation to describe twist-rate non-uniformity. To model the twist-rate non-uniformity, a twist-rate distribution function is defined. Let $P_{tr}(tr)$ be the actual probabilistic distribution of the twist rate tr of the real cable, and $P'_{tr}(tr)$ be the ideal probabilistic distribution of the

twist rate. The ideal twist-rate distribution is a delta function, $P'_{tr}(tr) = \delta(tr - \overline{tr})$, where $\overline{tr}$ is an expected twisted rate for the cable. In a real cable, the twist rate has a non-delta distribution function centered at the expected twist rate. Uniform and Rayleigh distributions for the twist rate are used in simulations to compare with measurement. For the uniform distribution, the following distribution $P_{tr}(tr)$ can be used:

$$P_{tr}(tr) = 1/2a, tr \in [\overline{tr} - a, \overline{tr} + a]. \tag{27}$$

For practical purposes, $a < 0.2 \cdot \overline{tr}$ can be chosen. For the Rayleigh distribution, $P_{tr}(tr)$ is given by:

$$P_{tr}(tr) = \frac{(tr) \cdot \exp(-(tr)^2 / (2 \cdot (\overline{tr})^2)}{(\overline{tr})^2}, \tag{28}$$

which has the largest value when $tr = \overline{tr}$. To simulate practical systems, overly short or long twist rates can be excluded. After selecting the twist-rate distribution function, the simulation software randomly picks twist rates according to the distribution function and arranges them along the cable until the complete cable length is reached. Partial twists may be needed at the end of the cable if full twists cannot exactly match the targeted cable length.

c) Type III Imperfection in Twisted pair Cables: Non-twisted Cable Head or Tail

In real cables, non-twisted tail and head sections may occur at connection points (ends of the cable). Even though the length of the cable tail or head section might be only a few centimeters (a very short length compared to a full cable length), simulations show that such short non-twisted sections may significantly affect the overall crosstalk level for the whole cable. This is because crosstalk from these non-twisting tail and head sections do not experience any cancellation.

III. Channel Characteristics and Numerical Examples

Based on the preceding circuit theory and cable geometry descriptions, the binder MIMO model can be used to calculate channel transfer functions for a binder or cable from basic system parameters. This section contains results for a few numerical examples and discusses general qualitative characteristics of these models of binder channels. These results are also compared with analytical predictions and

measured data. The main purpose of these examples is to verify the model. Since measured data are typically available only for differential excitations, this section focuses on examining the simulation results for differential excitation.

Due to their relative simplicity, crosstalk properties for "single quads" are presented first. Here, crosstalk is shown to be completely cancelled under normal differential excitation. The crosstalk properties for twisted pair cables are then presented with a focus on the effect of cable imperfections. The data shows that crosstalk is almost entirely cancelled for an ideal twisted pair cable but in a real cable, the pair-center variation and the twist-rate variation can greatly affect the crosstalk level. The simulations also show that cable imperfections have a substantial impact on crosstalk yet have a relatively small impact on the direct transfer function for a twisted pair. Results on how crosstalk depends on cable length will then follow. Simulation results are shown to match well with measured data.

A. Crosstalk for both Perfect and Imperfect Single Quads

For a perfect basic "single quad,", the centers of 4 wires form a square. The distances between the 4 wires are denoted as D-D-D-D where D is the diameter of a wire. For the cable, normal differential excitation is used to excite a pair of diagonal wires and crosstalk is measured over the other pair of diagonal wires; split-pair differential excitation excites two wires on the same side of a quad and crosstalk is measured over other two wires. It can be shown analytically that crosstalk under normal differential excitation is completely cancelled and the cancellation is caused by the perfect geometric symmetry of quad cables. If the symmetry is broken, the crosstalk cancellation mechanism of the diagonally excited quad is degraded. Fig. 4 shows crosstalk for a quad where the centers of 4 wires are slightly deviated from a perfect square. The distances of 4 wires are D-1.02D-D-1.02D (2% deviation from a square). Even with such small asymmetry, significant crosstalk under the normal differential excitation is clearly observed. More simulations show that for many practical cables, 2% deviation from a square works as a good approximation to compute crosstalk levels that match measurements.

B. Effects of Cable Imperfection on Crosstalk for Twisted pair Cables

Fig. 5 shows the effect of cable imperfections on FEXT and NEXT, as well as upon the direct transfer functions between two twisted pairs under normal differential excitation. Here, the normal

differential excitation is referred to as exciting two wires in the same twisted pair, and crosstalk is measured for another twisted pair. The length of the cable is 274 meters, and the type of the cable is 24 American wire gauge (AWG). The twist rate for one pair is 4.0inch (≈ 10.1centimeter) and for another pair, it is 6.2 inch (≈ 15.7 centimeter). A parallel layout is used for the simulation, and the expected distance between pair centers is 1.7mm. The figure shows results for 4 different scenarios: perfect twisting, with type III imperfection only (untwisted cable head and tail), with type III and type I imperfection (pair center variation), and with type III, I, and II (twist rate variation). Parameters used in describing imperfections are: 10% random pair-center variation, 3 cm untwisted cable head and tail, and uniform twist-rate distribution, where $P_{tr}(tr) = 1/2a, tr \in [\overline{tr} - a, \overline{tr} + a]$, $a = 0.15 \cdot \overline{tr}$. A few outstanding characteristics can be observed in this figure. First, without cable imperfection, both FEXT and NEXT are very small, which illustrates that the crosstalk is mostly cancelled for perfect twisted pairs, but this cancellation is not as complete as for the earlier example of the "quad" cables. This conclusion is analytically proved in [15]. Second, imperfections have a big impact on FEXT and NEXT levels; in particular, the twist-rate variation causes the NEXT to exhibit irregular patterns of notches and peaks over frequency. Third, the direct-pair transfer function is not significantly affected by imperfections. Even though these simulation results are obtained for the specific parameters used in this example, the general trends hold for other parameters. In general, simulation results suggest that for a twisted pair cable system, cable imperfections have great impact on crosstalk under normal differential excitation, but small impact on crosstalk under split-pair differential excitation [15]. Here, split-pair differential excitation is defined as follows: for two twisted pairs, a source is excited between two wires in different twisted pairs, and crosstalk is measured over the remaining two wires. Additionally, if non-differential excitation is used, such as the source and load impedances being matrix matched to the cable binder, cable imperfections are shown to have small impact on the crosstalk and direct-line transfer functions [15].

C. Crosstalks vs. Cable Length

This subsection presents how crosstalk depends on cable length, which had been reported as experimental and theoretical results in literature [23][23]. This subsection shows that the model and simulation presented in this work can also reveal a similar effect, further proving the usefulness of the

model. Fig. 6(a) shows an example of how NEXT and FEXT, as well as the direct pair transfer function, vary under the normal differential excitation when the cable length changes. This particular cable contains two pairs. The twist rates are 2.0 inch ($\approx 0.051m$) and 3.9 inch ($\approx 0.099m$) for each of two twisted pairs. The figure plots the average direct transfer function, NEXT, and FEXT over the frequency range of 0-20 MHz. In Fig. 6(a), the cable length changes from 274 to 274.2 meter. As expected, the direct transfer function remains almost constant when the cable length has such small variations. However, both NEXT and FEXT are very sensitive to the cable length variations, even though the variations are smaller than the twist rates. The effect, named here as the "Large Crosstalk Variations Due to Partial Twist", has been observed in measurements [9][17] and theoretically analyzed in [9][15]. The large crosstalk variations due to partial twist effect could have a considerable impact on the signal-to-noise ratio (S/N) for twisted pairs under the usual differential excitation when FEXT dominates other noises. Furthermore, simulation results suggest that this effect happens only under the normal differential excitation but not under split-pair differential excitation. Additionally, simulations show that a non-twisted cable head or tail can cause a similar effect. Fig. 6(b) shows a related but different effect. It shows how the direct-line transfer function and crosstalk vary with large cable length changes. The simulation uses same parameters as in Fig. 6(a) except that the cable length changes from 20 meters to 1200 meters. As can be seen from the figure, the direct transfer function monotonically decreases as the cable length increases, but the crosstalk does not decrease monotonically. The non-monotonic decrease of crosstalk is not all caused by the partial-twist effect. This is because the non-monotonic dependence on cable length is still observed even if the cable length is carefully chosen such that the partial twist is completely removed. Consequently, the S/N can vary by a few dB when the cable length increases. Therefore, a receiver closer to the source might have worse S/N than a receiver at a greater distance, with the usual differential excitation.

D. Simulation vs. Measured Data

Fig. 7(a) shows the measured values of the direct transfer function of a pair, NEXT and FEXT between two pairs in a real cable system. The cable consists of 25 twisted pairs (24AWG) of 274 meters length. The selected pairs are surrounded by neighboring pairs. The data was measured using a Network

Analyzer (Agilent 4395A); 50 to 100 Ohm baluns were used when needed. Fig. 7(b) shows the simulation results with 10% random pair-center variation and uniform twist-rate distribution, $P_{tr}(tr) = 1/2a, tr \in [\overline{tr} - a, \overline{tr} + a]$ where $a = 0.15 \cdot \overline{tr}$ are used. The simulation assumed two adjacent 24AWG pairs, each of length 274 meters. The two pairs are initially parallel. These two pairs are isolated in the air. 100 ohm source and load impedances are used in each pair. Physical constants $\mu, \varepsilon_r, \sigma$ (the permittivity, permeability and conductivity respectively) of the dielectric filling material of cables and resistance of cable are extracted [15]. They are all frequency dependent. The simulation results depend on the random-number generator (each random output of which of course represents a specific cable). The figure shows the result for one specific random number generator, which matches the measured data well suggesting that this particular random number is a good match to the specific cable. Note that the simulated FEXT is still "smoother" than measured data. The "roughness" of the measured FEXT can be caused by neighboring pairs and other cable imperfections, which were not included in the simulation.

The numerical results generated by the simulations in this paper depend on specific sets of cable parameters and in some cases, the random number generators. These results should be considered as more exploratory than definitive. In addition to the above examples, the binder MIMO model has been used to generate power sum for all crosstalk components in a cable binder, and simulation results have been compared with empirical results [12]. Results for practical achievable data rates using the common-mode MIMO channel are reported in [18]. The complete simulation software suites are available upon request.

IV. Conclusion

In this paper, a binder MIMO channel model is proposed to characterize the physical channels including all transfer functions and crosstalk couplings of multi-wire communication systems. The model is flexible in that it can accommodate various kinds of practical cables with different cable geometries, source-load configurations, and different types of cable imperfections. The model can be used not only to calculate NEXT and FEXT when a cable is used under (traditional) differential excitations, but also to calculate a MIMO channel matrix **H** when the system uses MIMO transmission methods. Once the channel matrix **H** is revealed, the achievable data rate of multi-wire communication systems can be

calculated**.** The model builds a relationship between the channel matrix **H** and the actual physical parameters such as source-load configurations, cable types, and geometry parameters; therefore, it can relate the achievable data rate with these parameters and provide helpful insights in real system designs. The proposed model does not include the effect of cable shielding or bridge taps, which are left for future work.

ACKNOWLEDGMENTS:

The authors wish to thank the reviewers and the associate editor for providing many constructive comments and suggestions, which have improved the quality of paper

REFERENCES

[1] T. Starr, M. Sorbara, J. M. Cioffi, P. J. Silverman, "DSL Advances," Prentice Hall, 2003.

[2] G. Ginis, J. M. Cioffi, "Vectored transmission for digital subscriber line systems," *IEEE Journal on Selected Areas in Comm.*, vol. 20, No. 5, pp. 1085-1104, June 2002.

[3] T. Starr, J. M. Cioffi, P. J. Silverman, "Understanding Digital Subscriber Line Technology", Prentice Hall, 1999.

[4] C. R. Paul, "Analysis of Multiconductor Transmission lines," John Wiley & Sons, 1994.

[5] S. O. Rice, "Steady state solutions of transmission line equations," *Bell Systems Techn. Journal*, pp. 131-178, Apr. 1941.

[6] S. Jagannathan, V. Pourahmad, K. Seong, J. M. Cioffi, M. Ouzzif, R. Tarafi, "Common-mode data transmission using the binder sheath in digital subscriber lines," submitted to *IEEE Trans. Commun.*, Feb. 2007.

[7] C. R. Paul and J. W. McKnight, "Prediction of crosstalk involving twisted pairs of wires —Part I: A transmission-line model for twisted-wire pairs," *IEEE Trans. Electromagnetic Compatibility*, vol. 21, pp. 92–105, May 1979.

[8] C. R. Paul, "Introduction to Electromagnetic Compatibility," Chapter 10, John Wiley & Sons, 1992.

[9] C. R. Paul and M. B. Jolly, "Sensitivity of crosstalk in twisted pair circuits to line twist," *IEEE Trans. on Electromagnetic Compatibility*, vol. 24, pp. 359–364, August 1982.

[10] D. Bellan, S.A. Pignari, G. Spadacini, "Characterisation of crosstalk in terms of mean value and standard deviation," *IEE Proceedings on Science, Measurement and Technology*, vol. 150, No. 6, Nov 2003.

[11] C. Valenti, "NEXT and FEXT models for twisted pair north American loop plant," *IEEE Journal on Selected Areas in Comm.*, vol. 20, No. 5, pp. 893-900, June 2002.

[12] J. Cioffi, B. Lee, M. Mohseni, M. H. Brady, K. Seong, Y. Kim, "Evolving channel modeling text for section 5.1 of DSM report," *ANSI Contribution T1E1.4/2003-033R2*, August 2003.

[13] Jeannie Lee, "Modeling and characterization of copper access systems," Ph.D. dissertation, Department of Electrical Engineering, Stanford University, Stanford, CA, 2002.

[14] J. A. B. Faria, M. V. G. das Neves, "Analysis of the helical twisted-wire pair running above ground: transfer function evaluation," *IEEE Trans. on Electromagnetic Compatibility*, vol. 45, No. 2, pp. 449-453, May 2003.

[15] Bin Lee, "Binder MIMO Channel," Ph.D. dissertation, Department of Electrical Engineering, Stanford University, Stanford, CA, 2004.

[16] M. B. Jolly and C. R. Paul, "Basic EMC technology advancement for C3 systems-crosstalk in twisted-wire circuits," Rome Air Development Center, Griffiss Air Force Base, NY, RADC-TR-82–286, vol. IV C, 1982.

[17] D. Joffe, "End effects on capacitance and inductance measurements in paired cable," *ANSI Contribution T1E1.4/2002-238*, Nov. 2002.

[18] B. Lee, J. Cioffi, S. Jagannathan, M. Mohseni, "Gigabit DSL", to appear *IEEE Trans. Commun*.

[19] N. Holte, "Calculation of Crosstalk in Balanced Pair Cables by means of Simulation," *Int. Wire and Cable Symp.*, Cherry Hill, USA, Nov. 1977.

[20] L. M. Wedepohl, "Application of matrix methods to the solution of travelling-wave phenomena in polyphase systems," *Proc. IEE*, vol 110, No 12, pp. 2200-2212, Dec. 1963.

[21] H. W. Friesen, "Relating the twist detection measurements of twisted pairs to their crosstalk performance," *Int. Wire and Cable Symp.*, Cherry Hill, USA, pp.150-157, Nov. 1975.

[22] H. W. Friesen, “Experimental verification of near end crosstalk equation for balanced telephone cable pairs,” *National Telecommunications Conference*, pp8C-1–11, Nov. 1973.

[23] T. A. Lenahan, “The theory of uniform cables–Part I: calculation of propagation parameters and Part II: calculation of charge components,” *Bell System Techn. Journal*, pp. 597-624, April 1977.

[24] N. Holte, “A Crosstalk Model for Cross-Stranded Cables,” *Int. Wire and Cable Symp.*,Cherry Hill, USA, Nov. 1982.

[25] H. Cravis, T. V. Crater, “Engineering of T1 carrier system repeatered lines,” *Bell System Techn. Journal*, vol.42, pp. 431-486, March 1963.

[26] A. J. Gibbs, R. Addie, “The covariance of near end crosstalk and its application to PCM system engineering in multipair cable,” *IEEE Trans. Commun.*, vol. COM-27, pp. 469-477, Feb. 1979.

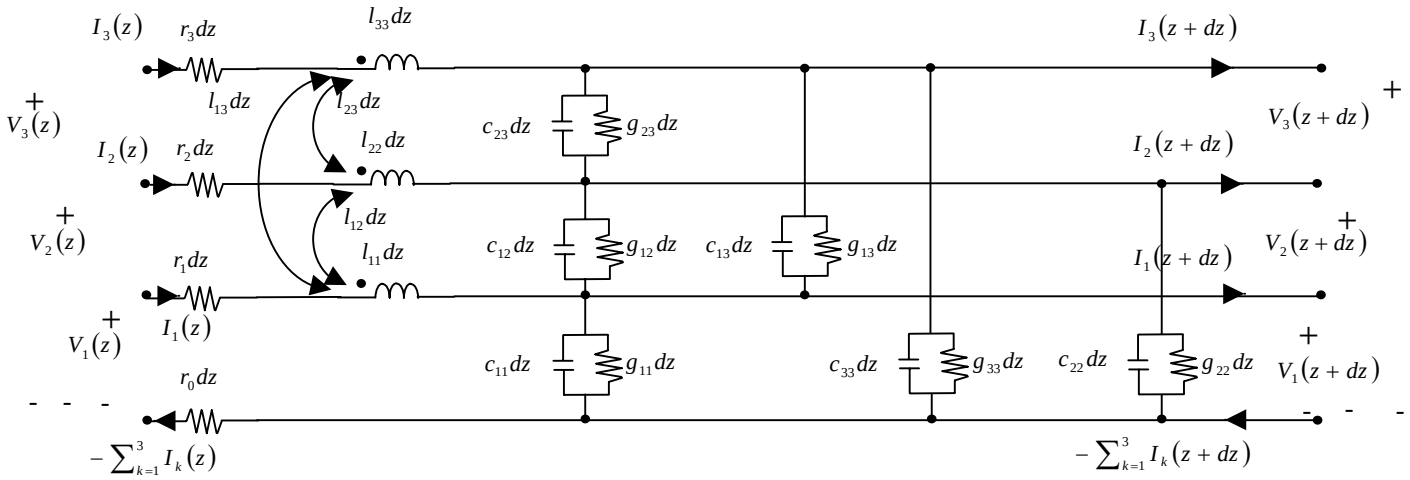

$$\mathbf{R}=\begin{bmatrix} r_0+r_3 & r_0 & r_0 \\ r_0 & r_0+r_2 & r_0 \\ r_0 & r_0 & r_0+r_1 \end{bmatrix} \quad \mathbf{L}=\begin{bmatrix} l_{33} & l_{23} & l_{13} \\ l_{23} & l_{22} & l_{12} \\ l_{13} & l_{12} & l_{11} \end{bmatrix} \quad \mathbf{C}=\begin{bmatrix} c_{13}+c_{23}+c_{33} & -c_{23} & -c_{13} \\ -c_{23} & c_{12}+c_{23}+c_{22} & -c_{12} \\ -c_{13} & -c_{12} & c_{13}+c_{12}+c_{11} \end{bmatrix}$$

$$\mathbf{G}=\begin{bmatrix} g_{13}+g_{23}+g_{33} & -g_{23} & -g_{13} \\ -g_{23} & g_{12}+g_{23}+g_{22} & -g_{12} \\ -g_{13} & -g_{12} & g_{13}+g_{12}+g_{11} \end{bmatrix}$$

Figure 1(a), A segment of cable binder can be described with **R**, **L**, ***C***, **G** and **V**, **I**

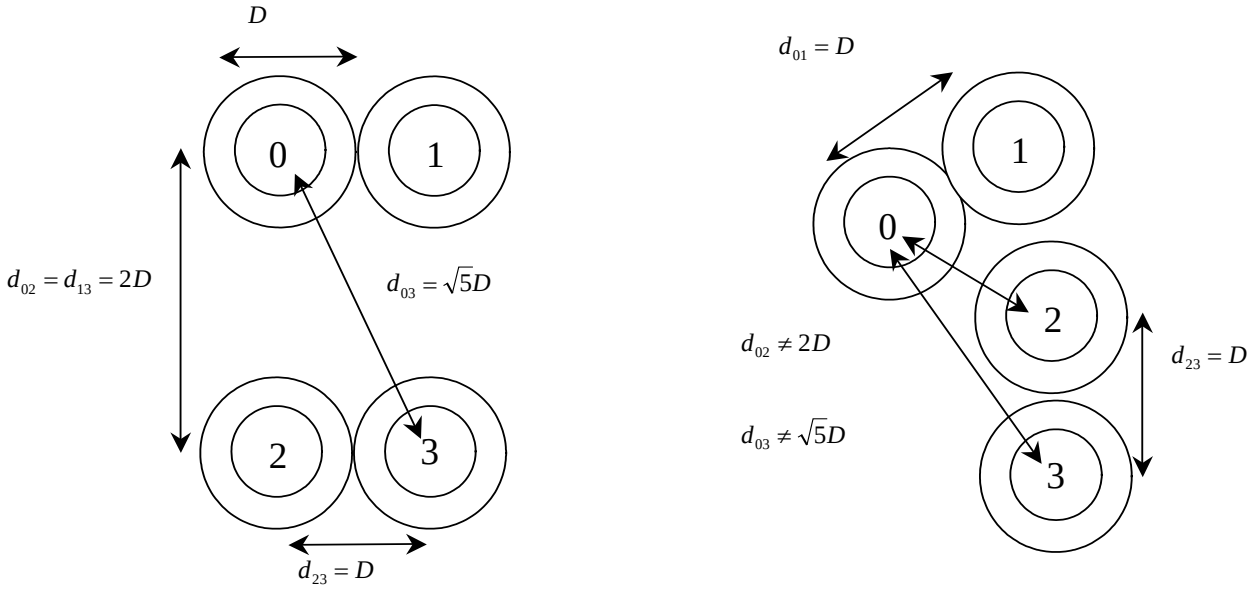

Figure 1 (b), Distance Between Pairs (and thus the **LCG** values) Varies with Twisting

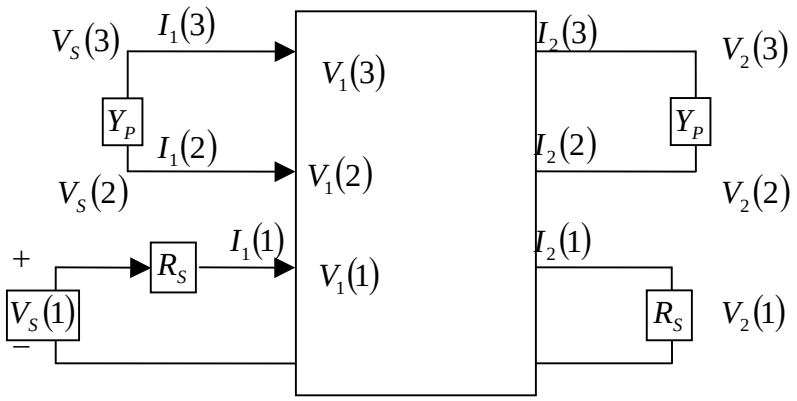

$$-\begin{bmatrix} I_1(3) \\ I_1(2) \end{bmatrix} = \mathbf{Y}_P \cdot \begin{bmatrix} V_1(3) \\ V_1(2) \end{bmatrix} \qquad \mathbf{I}_1 = \begin{bmatrix} \mathbf{I}_P \\ I_1(1) \end{bmatrix} \qquad \mathbf{V}_1 = \begin{bmatrix} \mathbf{V}_P \\ V_1(1) \end{bmatrix} \qquad \mathbf{I}_1 = \mathbf{Y}_1 \cdot \mathbf{V}_1 \qquad \mathbf{Y}_1 = \begin{bmatrix} \mathbf{Y}_{22} & \mathbf{Y}_{21} \\ \mathbf{Y}_{21}^T & Y_{11} \end{bmatrix}$$

$$-\mathbf{I}_P = \mathbf{Y}_P \cdot \mathbf{V}_P$$

Figure 2, Scalar Sources and Differential Loads

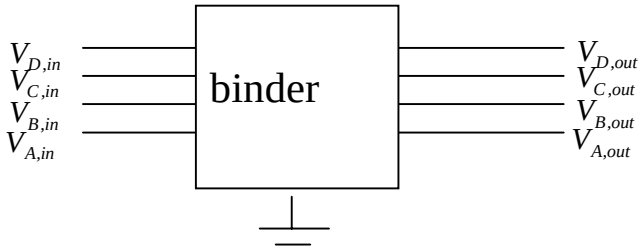

Absolute voltage model (w.r.t. earth/chassis ground)

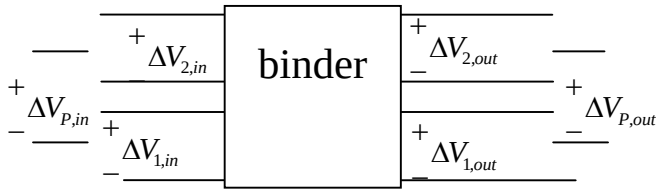

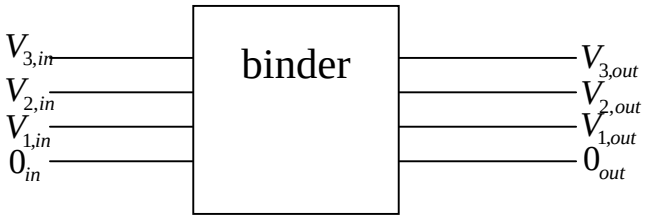

"Symmetric" model

"Asvmmetric" model

$$\Delta V_{1,in} = V_{B,in} - V_{A,in} = V_{1,in}$$
$$\Delta V_{2,in} = V_{D,in} - V_{C,in} = V_{3,in} - V_{2,in}$$
$$\Delta V_{P,in} = \left(\frac{V_{C,in}+V_{D,in}}{2}\right) - \left(\frac{V_{A,in}+V_{B,in}}{2}\right) = \left(\frac{V_{3,in}+V_{2,in}}{2}\right) - \frac{V_{1,in}}{2}$$

$$\begin{bmatrix} \Delta V_{P,in} \\ \Delta V_{2,in} \\ \Delta V_{1,in} \end{bmatrix} = \begin{bmatrix} .5 & .5 & -.5 \\ 1 & -1 & 0 \\ 0 & 0 & 1 \end{bmatrix} \cdot \begin{bmatrix} V_{3,in} \\ V_{2,in} \\ V_{1,in} \end{bmatrix}$$

$$0_{in} = V_{A,in}$$
$$V_{1,in} = V_{B,in} - V_{A,in}$$
$$V_{2,in} = V_{C,in} - V_{A,in}$$
$$V_{3,in} = V_{D,in} - V_{A,in}$$

$$\begin{bmatrix} V_{3,in} \\ V_{2,in} \\ V_{1,in} \end{bmatrix} = \begin{bmatrix} 1 & .5 & .5 \\ 1 & -.5 & .5 \\ 0 & 0 & 1 \end{bmatrix} \cdot \begin{bmatrix} \Delta V_{P,in} \\ \Delta V_{2,in} \\ \Delta V_{1,in} \end{bmatrix}$$

Figure 3, Equivalence of Traditional Symmetric Model and Asymmetric Model

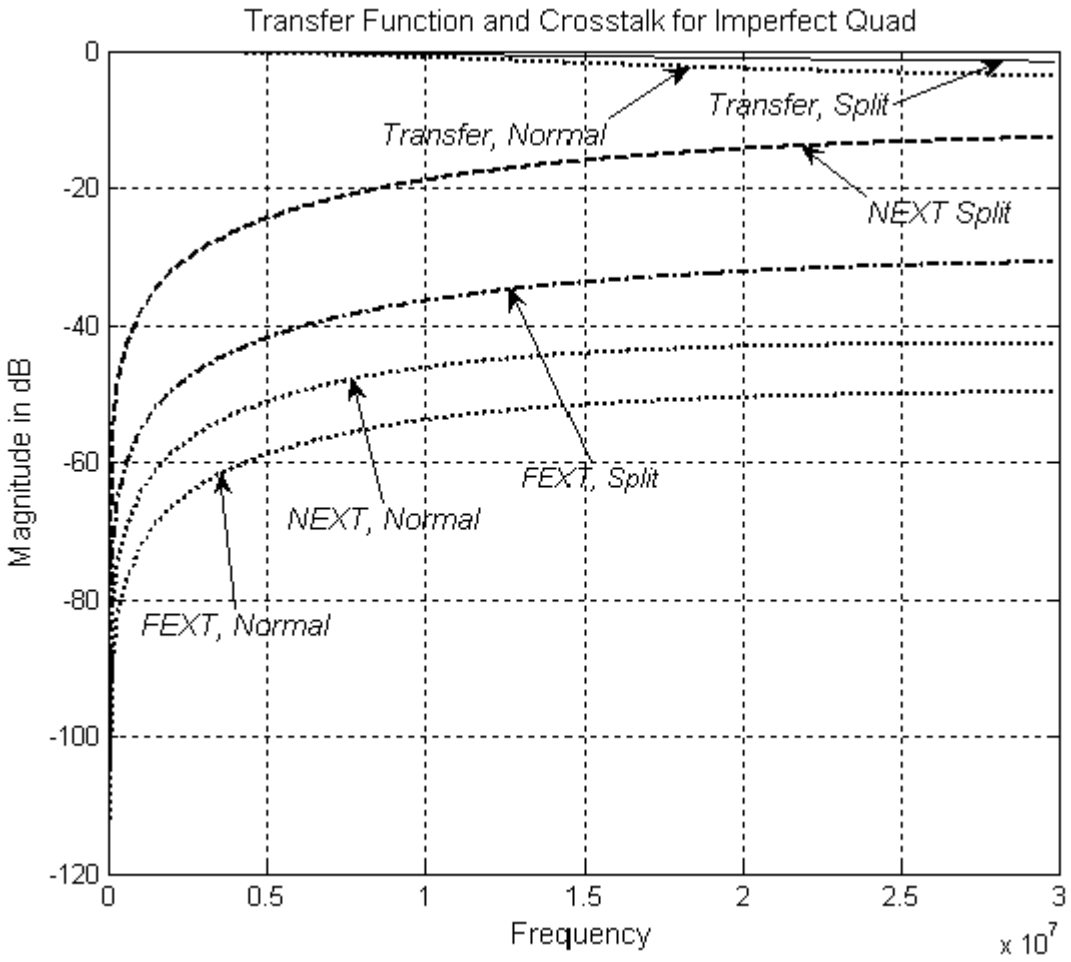

Figure 4, Crosstalk for 2 Meter Imperfect Quad Cable

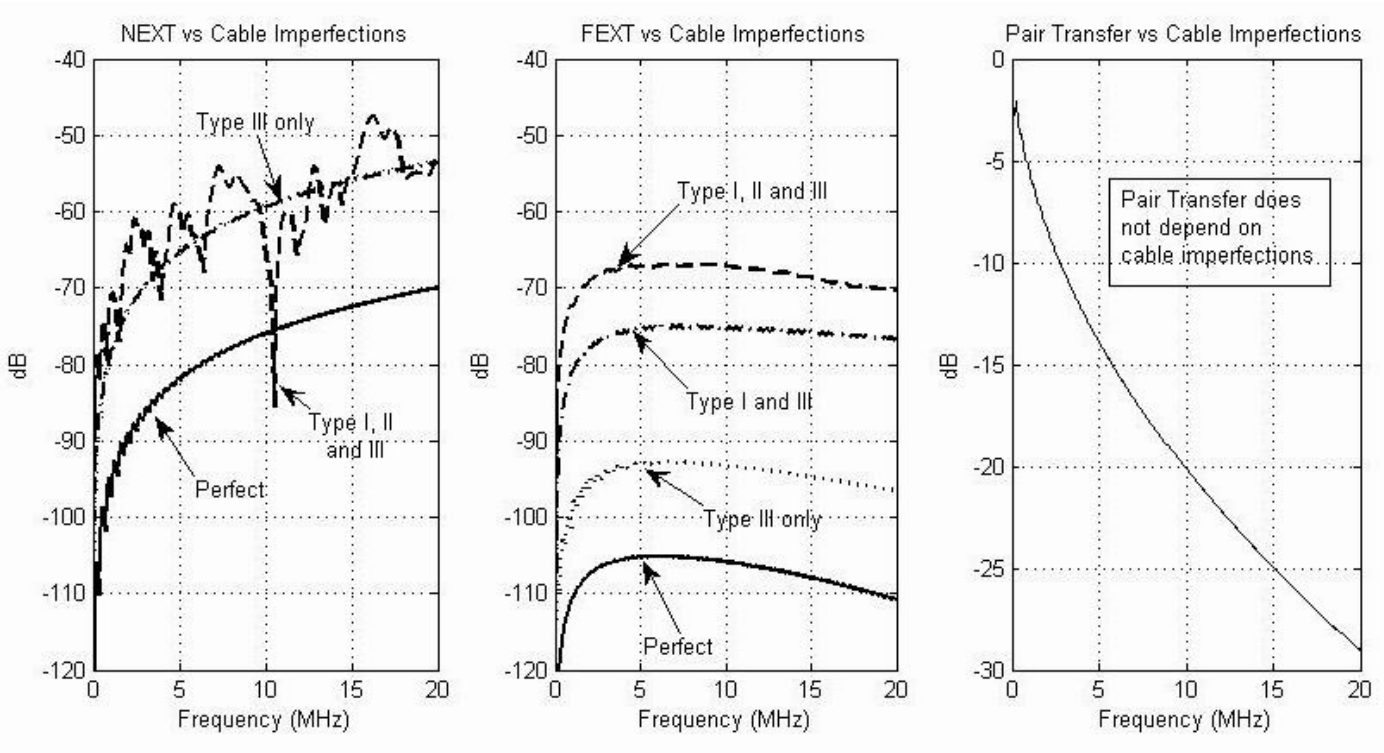

Figure 5, Effect of Cable Imperfection on Crosstalk under Normal Differential Excitation. 274 m, 24 AWG.

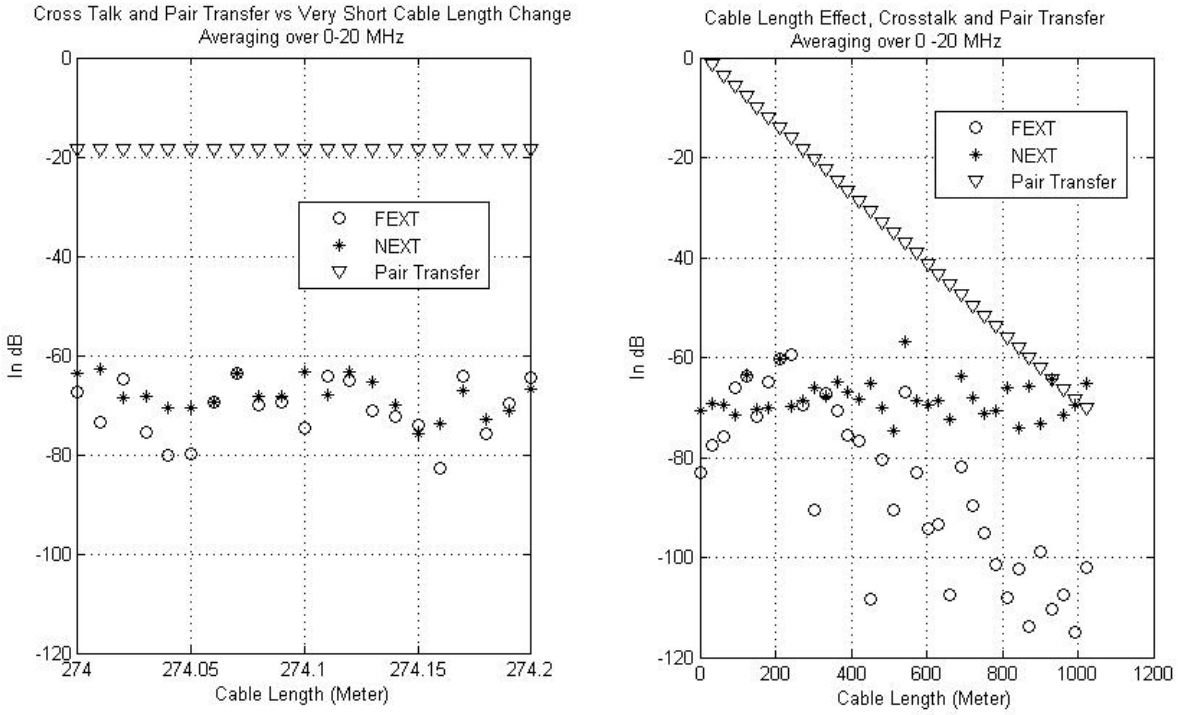

(a) (b)

Figure 6, Crosstalk as Function of Partial Twist and Cable Length

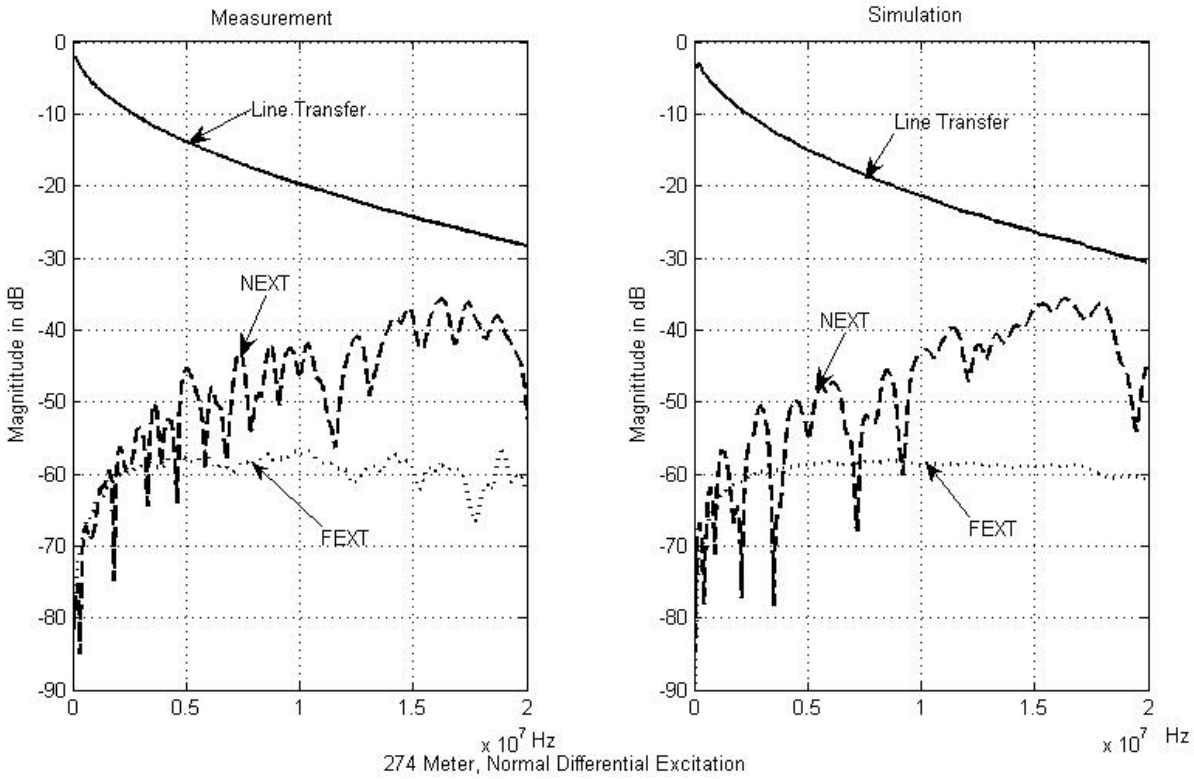

(a) (b)

Figure 7, Simulation vs. Measurement

Table 1
15 Transfer functions of interest for 3x3 Case – G is used for NEXT and H for FEXT
(first subscript is output and second subscript is input)

Label	Symmetric	Asymmetric
Direct transfer functions	$\frac{\Delta V_{1,out}}{\Delta V_{1,in}}$ $\frac{\Delta V_{2,out}}{\Delta V_{2,in}}$	$\frac{V_{1,out}}{V_{1,in}} = H_{11}$ $\frac{V_{3,out} - V_{2,out}}{V_{3,in} - V_{2,in}} = \frac{H_{32} - H_{22}}{G_{32} - 1}$
FEXT transfer functions	$\frac{\Delta V_{2,out}}{\Delta V_{1,in}}$ $\frac{\Delta V_{1,out}}{\Delta V_{2,in}}$	$H_{31} - H_{21}$ $\frac{H_{12}}{G_{32} - 1}$
NEXT transfer functions	$\frac{\Delta V_{2,in}}{\Delta V_{1,in}}$ $\frac{\Delta V_{1,in}}{\Delta V_{2,in}}$	G_{21} G_{12}
Phantom FEXT transfer functions	$\frac{\Delta V_{2,out}}{\Delta V_{P,in}}$ $\frac{\Delta V_{1,out}}{\Delta V_{P,in}}$ $\frac{\Delta V_{P,out}}{\Delta V_{2,in}}$ $\frac{\Delta V_{P,out}}{\Delta V_{1,in}}$	$\frac{2(H_{31} - H_{21})}{G_{31} + G_{32} - 1}$ $\frac{2(H_{11})}{G_{31} + G_{32} - 1}$ $\frac{H_{32} + H_{22} - H_{12}}{2(G_{32} - 1)}$ $\frac{H_{31} + H_{21} - H_{11}}{2}$
Phantom Direct transfer functions	$\frac{\Delta V_{P,out}}{\Delta V_{p,in}}$	$\frac{H_{31} + H_{21} - H_{11}}{G_{31} + G_{21} - 1}$
Phantom NEXT transfer functions	$\frac{\Delta V_{2,in}}{\Delta V_{P,in}}$ $\frac{\Delta V_{1,in}}{\Delta V_{P,in}}$ $\frac{\Delta V_{P,in}}{\Delta V_{2,in}}$ $\frac{\Delta V_{P,in}}{\Delta V_{1,in}}$	$\frac{2(G_{31} - G_{21})}{G_{31} + G_{32} - 1}$ $\frac{2}{G_{31} + G_{32} - 1}$ $\frac{G_{32} + G_{22} - G_{12}}{2(G_{32} - 1)}$ $G_{31} + G_{21} - 1$

Table 1, Results for Symmetric and Asymmetric Mode